A subset of platinum-containing chemotherapeutic agents kills cells by inducing ribosome biogenesis stress

HHS Public Access

Author manuscript

Nat Med. Author manuscript; available in PMC 2017 October 01.

Published in final edited form as:

Nat Med. 2017 April ; 23(4): 461–471. doi:10.1038/nm.4291.

A subset of platinum-containing chemotherapeutic agents kill cells by inducing ribosome biogenesis stress rather than by engaging a DNA damage response

Peter M. Bruno[1,2], **Yunpeng Liu**[1,2], **Ga Young Park**[3], **Junko Murai**[4], **Catherine E. Koch**[1,2], **Timothy J. Eisen**[2,5], **Justin R. Pritchard**[1,2], **Yves Pommier**[4], **Stephen J. Lippard**[1,3], and **Michael T. Hemann**[1,2]

[1]The Koch Institute for Integrative Cancer Research at MIT, Cambridge, MA 02139, USA

[2]Department of Biology, Massachusetts Institute of Technology, Cambridge, MA 02139, USA

[3]Department of Chemistry, Massachusetts Institute of Technology, Cambridge, MA 02139, USA

[4]Developmental Therapeutics Branch and Laboratory of Molecular Pharmacology, Center for Cancer Research, National Institutes of Health, Bethesda, MD 20892, USA

[5]Howard Hughes Medical Institute, Whitehead Institute for Biomedical Research, Cambridge, MA 02142, USA

Abstract

Cisplatin and its platinum analogues, carboplatin and oxaliplatin, are some of the most widely used cancer chemotherapeutics. However, although cisplatin and carboplatin are primarily used in germ cell, breast and lung malignancies, oxaliplatin is instead used almost exclusively in colorectal and other gastrointestinal cancers. Here, we utilize a unique multi-platform genetic approach to study the mechanism of action of these clinically established platinum anti-cancer agents as well as more recently developed cisplatin analogues. We show that oxaliplatin, unlike cisplatin and carboplatin, does not kill cells via the DNA damage response. Rather, oxaliplatin kills cells by inducing ribosome biogenesis stress. This difference in drug mechanism explains the distinct clinical implementation of oxaliplatin relative to cisplatin and may enable mechanistically informed selection of distinct platinum drugs for distinct malignancies. These data highlight the functional diversity of core components of front line cancer therapy and the potential benefits of applying a mechanism-based rationale to the use of our current arsenal of anti-cancer drugs.

Corresponding author statement: Michael Hemann (hemann@mit.edu) and Stephen Lippard (lippard@mit.edu).

Data Availability Statement

The data that support the findings of this study are available from the corresponding author upon reasonable request.

Author Contributions

P.M.B., Y.L., G.Y.P, T.J.E., J.R.P., D.P.B., Y.P., S.J.L and M.T.H. conceived the idea for the research, designed experiments and interpreted data. P.M.B., Y.L. and C.E.K. performed experiments. P.M.B. and Y.L. performed bioinformatic analyses. J.M. performed DT40 sensitivity profiles. T.J.E. performed polysome gradient profiling. P.M.B., S.J.L. and M.T.H. wrote the paper.

Competing Financial Interests Statement

The authors declare no competing financial interests.

The use of cisplatin in the clinic began over 45 years ago in the absence of understanding of the cellular and molecular mechanisms that underlie its efficacy[1]. Despite this, cisplatin has become a component of treatment regimens for at least 18 distinct tumor types[2]. However, cisplatin-induced side effects and the emergence of resistance to treatment led to the development of two derivatives, carboplatin and oxaliplatin, which have also seen considerable clinical use in a wide array of cancers. Interestingly, oxaliplatin has a different side effect profile than cisplatin and carboplatin, and it is used in colorectal and other gastrointestinal cancers where cisplatin and carboplatin have minimal efficacy. However, the decision to use oxaliplatin to treat colorectal cancer was primarily motivated by its activity against colorectal cancer cell lines in the human tumor cell line panel known as the NCI-60 and not due to a rationale involving its mechanism of action[3,4]. Although the assumption has been that oxaliplatin, like cisplatin, kills cells by eliciting a DNA damage response, no satisfactory explanation for oxaliplatin's unique clinical use and side effect profile has been identified. Here, we demonstrate that oxaliplatin acts through a fundamentally distinct mechanism of action relative to cisplatin and we propose that these agents should be used in a mechanism-targeted manner in the treatment of cancer.

Results

Diverse mechanisms of action for platinum compounds

To examine the mechanism of action of cisplatin and its platinum analogues we used an RNAi-based functional genetic strategy to predict mechanism of cytotoxic drug action[5–7]. This methodology has the advantages of being mammalian, isogenic and unbiased by dosage effects resulting from export or metabolism. Additionally, it has previously been used to characterize the mechanism of action of other metal based anti-cancer agents[8–15]. It is based on a fluorescence competition assay using lymphoma cells that are partially infected with eight short hairpin RNAs (shRNAs) that target distinct genes encoding proteins with known or putative roles in cell death signaling pathways: p53 (*TP53*), Chk2 (*CHEK2*), Chk1 (*CHEK1*), ATR (*ATR*), ATX (*SMG1*), DNAPKcs (*PRKDC*), Bok (*BOK*) and Bim (*BCL2L11*). The shRNA-bearing cells either enrich or deplete relative to the uninfected population based on the survival advantage or disadvantage conferred by a given shRNA (Fig. 1a). The combined responses of these cells to different drugs constitute drug "signatures". Signatures of all classes of clinically used cytotoxic agents have been generated and assembled into a reference set separated into eight distinct categories of drugs based on the constituents' shared molecular mechanism of action (Supplementary Table S1). A new drug signature can then be classified by a probabilistic K-nearest neighbors algorithm to determine whether a new drug belongs to a class in the reference set or requires a new category not represented therein (Fig. 1b).

To eliminate dosage or potency effects from confounding the RNAi signatures, all agents were administered at a concentration that killed 80–90% (LD80–90) of the cells at 48 h. These LD80–90 concentrations varied greatly from one compound to the next (Supplementary Fig. 1a). However, via atomic absorption spectroscopy we determined that for cisplatin analogues representing low, medium and high potency, the amount of platinum required inside the cells for killing corresponded to their respective LD80–90 values

(Supplementary Fig. 1b). For instance, pyriplatin treatment at LD80–90 lead to much more intracellular platinum than the other LD80–90 treatment, indicating each molecule is relatively less toxic. Thus, differences in cellular uptake were effectively controlled using LD80–90 concentrations.

Next, to examine the mechanism of action of cisplatin, carboplatin and oxaliplatin we obtained their RNAi signatures. As expected, cisplatin and carboplatin were both predicted to be DNA cross-linkers (Fig. 1c,d, Supplementary Table S2, and Supplementary Fig. S2a). Previously, the three FDA-approved platinum based drugs had been understood to function primarily as DNA damaging agents that form intra- and interstrand cross-links. These cross-links are, in turn, removed largely by excision repair, generating single or double-stranded breaks in the process[16]. However, despite the fact that oxaliplatin putatively forms 1,2-intrastrand and other cross-links on DNA, oxaliplatin classified as being most similar to compounds that inhibit transcription or translation (Fig. 1c,d, Supplementary Table S2, and Supplementary Fig. S2a). These data may begin to explain why oxaliplatin has a different cytotoxicity profile and clinical application. Additionally, RNAi signatures of cisplatin and oxaliplatin taken in combination with 5-fluorouracil (5-FU), the primary drug with which oxaliplatin is paired with, preserved these mechanistic differences (Supplementary Fig. 3). Prior analysis of NCI-60 data similarly concluded that oxaliplatin acts distinctly relative to cisplatin and carboplatin, although no cellular function was identified as being responsible for the difference[17]. Notably, in this prior study, compounds clustered strictly by structure which is indicative of the NCI-60 methodology's emphasis on drug metabolism and transport over mechanism of action[18].

Interestingly, phenanthriplatin, a monofunctional and highly potent platinum(II) compound, also classified as a transcription/translation inhibitor (Fig. 1c,d, Supplementary Table S2, and Supplementary Fig. S2c). Because phenanthriplatin is incapable of making DNA cross-links, yet also classifies as a transcription/translation inhibitor like oxaliplatin, it suggests that the ability of oxaliplatin to form cross-links on the DNA is irrelevant to its mechanism of action. We went on to characterize seven additional platinum compounds and discovered that most also classified as DNA cross-linkers or transcription/translation inhibitors (Supplementary Fig. S2b,c and Supplementary Table S2). Curiously, two monofunctional platinum agents, acriplatin and pyriplatin, were found to have mechanisms of action not represented in our reference set (Supplementary Fig. S2d and Supplementary Table S2). This suggests that potential mechanisms of action for platinum compounds extend beyond the scope of anti-cancer agents in current clinical use. Furthermore, these signature predictions are maintained in all permutations of leave-one-out cross-validation of the drugs in the reference set (Supplementary Table S3). Additionally, we used an indicator of structural similarity, the Tanimoto coefficient[19], to hierarchically cluster the compounds and found that structural clustering was unable to recapitulate RNAi signature-based clustering, regardless of whether the compounds were clustered by their native structure or their anticipated structure once inside the cell (Supplementary Fig. S4). Thus, mechanism cannot be correctly predicted based on structure alone.

To more thoroughly examine the differences in RNAi signatures used to classify these molecules, we performed a detailed analysis of all of their signatures. The most notable

differences included decreased resistance with shChk2 and decreased sensitivity with shChk1 for the transcription/translation inhibitor-like compounds relative to the DNA cross-linker-like compounds (Fig. 1e and Supplementary Table 4). As another means of visualizing the data, we utilized principal components analysis (PCA) to represent the variance of our data in fewer dimensions. Plotting all of our tested platinum analogues with canonical transcription/translation inhibitors, DNA cross-linking agents, and Top2 poisons, we saw that the transcription/translation inhibitors separated from DNA cross-linkers along the first principal component (PC1) (Fig. 1e). Upon examining the variable contributions that made up PC1, we saw that shChk2 contributed most strongly among the hairpins. We also identified Chk2 as the greatest contributor to the distinction between these two sets of drugs in a p185+ *BCR-Abl p19*$^{arf-/-}$ mouse model of acute lymphoblastic leukemia (ALL)[20] (Supplementary Fig. S2e,f).

DNA damage response affects response to cisplatin but not oxaliplatin

To confirm the RNAi signature data using a parallel approach, we examined drug response in the avian DT40 cell line[21]. Here, 40 different DT40 cell lines, each with a different gene knockout related to DNA damage repair and tolerance, were dosed with five different platinum agents. In agreement with our RNAi signatures, the DT40 knockouts showed distinct sensitivities to oxaliplatin and phenanthriplatin relative to the other three platinum agents (Fig. 2a,b, and Supplementary Tables S5–6). In particular, loss of genes involved in homologous recombination (HR) (*XRCC2*, *XRCC3*, *BRCA2*) and interstrand cross-link repair (ICR) (*FANCC*, *FANCD2*, *FANCG*) showed the greatest differences between the two categories of platinum agents. The relative lack of sensitivity of HR and ICR deficient cells to oxaliplatin suggests that it, like phenanthriplatin, fails to form intra- and interstrand cross-links. Interestingly, genes necessary for replication bypass (*POLZ* and *PCNA*) were critical for all of the platinum derivatives. This result suggests that oxaliplatin and phenanthriplatin treatment create lesions on the DNA that are only toxic in the absence of normal replication bypass machinery. In addition, these results were recapitulated using RNAi against several genes related to DNA damage repair and/or tolerance in *Eμ-Myc p19*$^{Arf-/-}$ lymphoma cells and in *Eμ-Myc p53*$^{-/-}$ lymphoma cells (Supplementary Fig. S5a,b). Thus, relative drug sensitivities in the context of DT40 knockout cells support the RNAi-based category classifications.

Dependency on checkpoint kinases stratifies platinum agents

Given the importance of the two cell cycle checkpoint kinases, Chk1 and Chk2, in discriminating between the two mechanistic classes of platinum drug action and DNA damage response signaling, we decided to first confirm that these distinctions are relevant *in vivo.* To do this, we conducted a cell competition experiment using the *Eμ-Myc p19*$^{Arf-/-}$ lymphoma cells that were partially infected with GFP-tagged shChk2 and then tail-vein injected into syngeneic recipient mice. Tumors from untreated, cisplatin, oxaliplatin or phenanthriplatin treated mice were then analyzed for GFP percentage. As the *in vitro* data predicted, shChk2-containing cells significantly enriched compared to uninfected cells in mice treated with cisplatin but not in mice treated with oxaliplatin or phenanthriplatin (Fig. 3a). These results suggest that dependence on Chk2 activity, a key mediator of the canonical

DNA damage response, represents a primary distinction between the mechanistic classifications of DNA cross-linkers and transcription/translation inhibitors.

Subsequently, we examined the cell cycle profiles of cells treated with phenanthriplatin, oxaliplatin, and cisplatin treatment for 12 h at LD80–90. Oxaliplatin and phenanthriplatin induced a G1 cell cycle arrest whereas cisplatin arrested cells in the S and G2/M phases (Fig. 3b). We obtained similar results with the three drugs after 24 h of treatment in human lung adenocarcinoma and colorectal cell lines, A549 and LoVo, respectively (Supplementary Fig. S6). To determine the mechanistic basis for these cell cycle differences, we examined signaling pathways that may be engaged following induction of the DNA damage response. As shown by western blot, p21 (*CDKN1A*) protein is activated more quickly in response to oxaliplatin and phenanthriplatin than cisplatin (Supplementary Fig. S7a). Additionally, knockdown of p21 sensitizes cells to oxaliplatin and phenanthriplatin treatment but elicits resistance to cisplatin (Supplementary Fig. S7b).

Next, to gain further insight into DNA damage signaling in response to these compounds, we examined the p53 activating kinase, Chk2. Chk2 is activated in response to double-strand breaks, whereby it goes on to phosphorylate p53 on serine 20 (serine 18 in mice), which relieves MDM2 inhibition of p53[22]. Thus, treatment of cells with DNA damaging agents selects for cells harboring Chk2 or p53 hairpins. Consequently, mechanistic characteristics of DNA cross-linking agents should be discernible by examining canonical markers of DNA damage. We therefore tested for γ-H2AX and phosphor-ser18 p53 by Western blot at 12 h with and without hairpins targeting Chk1 and Chk2 for cisplatin, oxaliplatin and phenanthriplatin. We observed that treatment with oxaliplatin and phenanthriplatin resulted in γ-H2AX signal, but this was not dependent on Chk2, as it was for cisplatin (Fig. 3c). All three drugs also elicited total p53 induction and phosphorylation of p53; however, this was dependent on Chk2 for cisplatin (Fig. 3d). Additionally, the same was observed for both γ-H2AX and p53 at 4 h comparing cisplatin and phenanthriplatin with and without shChk2 (Supplementary Fig. S8a,b). Moreover, we observed upregulation of p53 transcriptional targets Puma and Noxa following phenanthriplatin treatment, concomitant with the increase in p53 levels seen by western blot (Fig. 3e). Subsequently, we examined γ-H2AX and phospho-ser18 p53 at and prior to 4 h. Phenanthriplatin, and to a lesser degree oxaliplatin, induced γ-H2AX, phosphor-ser18 p53 and total p53 accumulation, sooner and to a greater degree than cisplatin (Supplementary Fig. S8c,d). Phenanthriplatin and oxaliplatin also caused more rapid cell death than cisplatin and doxorubicin (Supplementary Fig. S9). We confirmed that cisplatin-induced phosphorylation of serine 20 of p53 was Chk2 dependent in the human LoVo colorectal cell line (Supplementary Fig. S10a). Furthermore, the transcript levels of the pro-apoptotic gene, Noxa, were increased following treatment with all platinum agents tested in multiple human cell lines (Supplementary Fig. S10c–e). Taken together, the early activation of apoptosis along with the early appearance, persistence, and Chk2 independence of γ-H2AX and phospho-ser18 p53 suggest a mechanism of cell death induced by oxaliplatin and phenanthriplatin that does not rely on canonical DNA strand-break signaling.

Oxaliplatin does not induce a DNA damage response

Considering the aforementioned rapid induction of γ-H2AX signal and early apoptosis following oxaliplatin and phenanthriplatin treatment, we examined γ-H2AX via immunofluorescence in order to distinguish DNA damage-related foci from pan-nuclear γ-H2AX; the latter is indicative of apoptosis[23,24]. We observed, as expected, that cisplatin-treated cells had γ-H2AX foci characteristic of a DNA damage response. However, similar to untreated cells, oxaliplatin and phenanthriplatin treated cells did not have γ-H2AX foci (Fig. 4a–d). Quantification of γ-H2AX signal showed that at both 4 and 8 h, nearly all of the γ-H2AX signal in oxaliplatin and phenanthriplatin-treated cells was derived from pan-nuclear γ-H2AX (Fig. 4c). Additionally, in the human LoVo cell line we confirmed that oxaliplatin-treated cells had significantly fewer γ-H2AX foci compared to cisplatin-treated cells (Supplementary Fig. S10f).

To further explain the absence of a DNA damage response following treatment with oxaliplatin and phenanthriplatin, comet assays were performed 6 h after treatment. Comet assays test for the presence of smaller weight DNA fragments produced following DNA breaks. A neutral comet assay, most sensitive to DNA double-strand breaks, indicated that oxaliplatin and phenanthriplatin treatment results in significantly fewer double-strand breaks than untreated or cisplatin treated murine lymphoma or human breast cancer cells (Fig. 4e and Supplementary Fig. S10g). Interestingly, an alkaline comet assay, sensitive to both single and double-strand breaks, indicated that only oxaliplatin treatment yielded significantly fewer DNA breaks than either no treatment or cisplatin treatment (Fig. 4f). It has been previously shown that in the alkaline comet assay S-phase cells yield longer tails than G1 or G2 cells. This result is consistent with having a large proportion of cells in S-phase as in the untreated condition, particularly relative to oxaliplatin and phenanthriplatin treatment[25].

Oxaliplatin and phenanthriplatin induce ribosome biogenesis stress

Our RNAi signatures predicted the mechanism of action of oxaliplatin and phenanthriplatin to involve transcription or translation inhibition. To further explore this possibility, we first measured the amount of platinum on RNA and DNA after 3 h of cisplatin, oxaliplatin and phenanthriplatin treatment at LD80–90. Atomic absorption spectroscopy revealed that all three compounds were present at appreciable amounts on both nucleic acids (Fig. 5a). Interestingly, oxaliplatin treatment yielded the least amount of platinum on either nucleic acid - potentially because it has the lowest LD80–90 concentration.

Defects in ribosome biogenesis can rapidly induce cell death in a p53-dependent and DNA damage-independent manner[26]. Given the similarity between this type of cell death and that induced by oxaliplatin and phenanthriplatin treatment, we examined ribosomal RNA (rRNA) synthesis following drug treatment. Indeed, we observed that within 30 minutes, pre-rRNA was decreased by nearly 50% in response to oxaliplatin and phenanthriplatin treatment (Fig. 5b). At later time points, pre-rRNA was upregulated many-fold by oxaliplatin and phenanthriplatin exposure – a phenotype paralleled by actinomycin D, a known inducer of ribosome biogenesis stress[26], but not cisplatin (Fig. 5b). Importantly, RNA polymerase II transcript levels were unaffected by treatment with any of the platinum agents

(Supplementary Fig. S11). Finally, to demonstrate on a functional genetic level that ribosome biogenesis stress was relevant to cell death caused by oxaliplatin and phenanthriplatin, we examined the role of RPL11 (*RPL11*) in drug-induced cell death. Ribosome biogenesis stress results in excess subunits of RPL11 that then bind Mdm2 and block the ability of Mdm2 to bind p53[26]. shRNA-mediated knockdown of RPL11 in Eu-Myc $p19^{Arf-/-}$ lymphoma cells and A549 human lung adenocarcinoma cells confers resistance to agents that induce ribosome biogenesis stress, including actinomycin D, rapamycin, mithramycin A, BMH-21 and 5-FU (Fig. 5c and Supplementary Fig. S12a–c). shRPl11 also induced resistance to oxaliplatin or phenanthriplatin treatment. Furthermore, we examined total p53 and cleaved Poly-ADP ribose polymerase 1 (cPARP) levels with or without an RPL11 hairpin 12 h after treating with the platinum agents and actinomycin D (Fig. 5d and Supplementary Fig. S12d). We saw that RPL11 knockdown led to diminished total p53 and cleaved PARP1 levels in cells treated with actinomycin D, oxaliplatin or phenanthriplatin, but not cisplatin. This effect is particularly strong when accounting for p53 and cPARP induction caused by knockdown of an essential component of the ribosome such as RPL11. Thus, the ribosome biogenesis stress pathway is a central mediator of oxaliplatin and phenanthriplatin cytotoxicity.

The localization of nucleolar proteins is altered in a characteristic manner in response to different types of cellular stress[27], including impaired translation. After 8 h of treatment *Eu-Myc* $p19^{Arf-/-}$ lymphoma cells with the platinum agents and actinomycin D, we observed differences in the localization of nucleophosmin and fibrillarin, two proteins normally localized to the nucleolus (Supplementary Fig. S13a). Cisplatin treatment did not result in any cells with nucleolar foci whereas actinomycin D, oxaliplatin and phenanthriplatin treatment resulted in a modest increase relative to no treatment (Supplementary Fig. S13b). More notably, nucleophosmin was predominantly found outside the nucleus for roughly 80 percent of cisplatin treated cells, but not in the other conditions (Supplementary Fig. S13c). The unique localization of nucleolar proteins among platinum agents further indicates that oxaliplatin and phenanthriplatin have a mechanism of action that is distinct from cisplatin and more similar to actinomycin D.

Next we sought to gain more insight into the influence oxaliplatin may exert on translation machinery. To do so, we first examined the polysome profiles of *Eu-Myc* $p19^{Arf-/-}$ lymphoma cells after 6 h of treatment with cisplatin, oxaliplatin and phenanthriplatin. Cells treated with oxaliplatin or phenanthriplatin had significantly fewer polysomes relative to monosomes compared to untreated or cisplatin treated cells (Fig. 5e,f and Supplementary Fig. S14). Thus, the global translation machinery is significantly perturbed by oxaliplatin treatment. Next, to more directly demonstrate the potential disruptive effect oxaliplatin treatment had on translation, we quantified nascent protein synthesis via a click-chemistry compatible puromycin analogue[28]. Indeed, we observed in multiple cancer cell lines that oxaliplatin disrupts protein synthesis as early as 9 h after treatment (Fig. 5g and Supplementary Fig. S15).

If oxaliplatin impairs ribosomal function, we would expect to see an effect of oxaliplatin treatment on the efficacy of known translation inhibitors. To examine this possibility, we treated cells with a combination of rapamycin, an mTOR inhibitor and known ribosome

biogenesis stress inducer, and either cisplatin or oxaliplatin. We then measured synergy or antagonism by comparing to the Bliss Independence additivity model[29]. We saw that the combination of cisplatin and rapamycin was additive, as indicated by the near zero deviation from Bliss Independence (Fig. 5h). However, the combination of oxaliplatin and rapamycin was very antagonistic. Interestingly, this antagonism was not present if oxaliplatin was dosed before rapamycin, indicating an epistatic relationship between the mechanisms of action of the two drugs (Fig. 5i). To further study this relationship, we examined RNAi signatures to understand how the mechanisms of action varied in combination. Interestingly, the signature was more similar to rapamycin alone than oxaliplatin alone whether dosed simultaneously or dosed with oxaliplatin 6 h prior to rapamycin (Fig. 5j). This suggests that active translation must be occurring in order for oxaliplatin to exert its cytotoxic effects.

Ribosome biogenesis stress sensitizes cells to oxaliplatin

Next, we sought to determine if ribosome biogenesis stress was a central determinant of oxaliplatin efficacy in human cells and across diverse tumor types. To perform this analysis, we utilized the NCI-60 human cancer cell line database, which includes gene expression data for each cell line and their oxaliplatin treatment response. Using the CellMiner NCI-60 database query tool[30], we were able to probe for genes whose expression in naïve cells correlated to sensitivity to oxaliplatin treatment. For example, *RSL24D1,* the gene most highly correlated to sensitivity is shown in comparison to drug response profile of oxaliplatin (Fig. 6a and Supplementary Fig. S16). By performing gene ontology annotation via DAVID on the list of 417 genes whose expression significantly correlated with oxaliplatin sensitivity, we identified an enrichment of terms related to translation, the ribosome and rRNA (Fig. 6b)[31,32]. Additionally, Gene Set Enrichment Analysis (GSEA) on the same set of genes identified “ribosome” as the only significantly enriched KEGG pathway (Fig. 6c)[33]. Performing similar analysis for cisplatin at the same threshold used for oxaliplatin only yielded one gene, *SFLN11.* Whereas the previous analysis examined gene expression relative to the entire set of cell lines, we wanted to see if expression of translation machinery correlated with oxaliplatin sensitivity within particular cancer types. Indeed, we saw that in both lung and breast cancer cell lines, higher translation machinery expression correlated with an increase in oxaliplatin sensitivity (Fig. 6d).

We reasoned that this increased expression of translation machinery represents a “translation addiction” and that ribosome biogenesis stress inducers kill by depriving the cell of translation machinery. Thus, a further increase of translation machinery expression would buffer against translation machinery depriving treatments such as ribosome biogenesis stress inducers. To examine this, we knocked down PTEN (*PTEN*) in order to upregulate the mTOR pathway and thus elevate translation machinery expression (Supplementary Fig. S17). Indeed, upon knocking down PTEN, the cells were rendered more resistant to known ribosome biogenesis stress inducers actinomycin D and 5-FU, as well as to oxaliplatin (Fig. 6e). Interestingly, we also saw that PTEN knockdown sensitized to cisplatin.

We next wanted to explore how these results might be relevant to the clinic. Given the frequent use of oxaliplatin in the treatment of colorectal cancer, we examined whether translation addiction could underlie oxaliplatin efficacy in this disease as opposed to cancers

where oxaliplatin shows little efficacy. We compared gene expression between all available colorectal and ovarian tumor samples from the The Cancer Genome Atlas (TCGA)[34,35]. We then performed GSEA on all differentially expressed genes between the two cancer types. Based on genes that are upregulated in colorectal cancer relative to ovarian cancer, GSEA identified the “ribosome” as one of the most enriched pathways that distinguishes colorectal cancer from ovarian cancer (Fig. 6f and Supplementary Table S7). GSEA did not identify any significant pathway enrichment from genes upregulated in ovarian cancer relative to colorectal cancer (Supplementary Table S8). Collectively, these data argue that the efficacy and clinical utility of oxaliplatin is derived from its ability to induce ribosome biogenesis stress.

Finally, we wanted to determine if we could identify correlates of oxaliplatin response in cancers that are not typically thought to respond to oxaliplatin. Prior studies have indicated that APC (*APC*), a key negative regulator of the Wnt pathway, loss in colorectal cancer causes a “translation addiction” that is necessary for tumorigenesis[36]. Thus, we examined Wnt pathway genes and their correlation to translation metagene expression in the TCGA expression databases[37]. Interestingly, we found that APC expression significantly correlated with translation metagene expression in several cancers, including breast and lung (Fig. 6g and Supplementary Fig. S18). We chose breast cancer for further examination as the NCI-60 breast cancer cell lines had the best correlation between translation machinery expression and oxaliplatin sensitivity. Using a panel of breast cancer cell lines, we confirmed that APC expression correlated with oxaliplatin sensitivity (Fig 6h). Therefore, APC expression may represent a marker of oxaliplatin sensitivity in breast cancers, and potentially other cancers as well.

Discussion

Our findings have significant implications for the evaluation of small molecules and their derivatives used in the clinic. First, in addition to potential changes in drug pharmacodynamics and pharmacokinetics, alterations in the nature of the ligands in platinum complexes have profound implications for primary mechanism of action. Thus, platinum drugs may not function interchangeably with their derivatives in cancer regimens. This phenomenon explains a lack of efficacy for oxaliplatin in the treatment of malignancies conventionally treated by cisplatin, as well as the unanticipated and poorly understood value of oxaliplatin as a treatment for colorectal cancer[38–41]. Second, changes in small molecule structure can alter the molecular determinants of chemotherapeutic response. For example, instead of cisplatin, oxaliplatin has been tested as a front-line treatment for breast and non-small-cell lung cancer (NSCLC)[42–47]. Furthermore, recent sequencing data has shown that greater than ten percent of breast and non-small cell lung cancers harbor inactivating mutations in *ATM* and Chk2[48,49]. Our data suggest that these mutant tumors may have differential responses to cisplatin versus oxaliplatin. Thus, tumor mutations may represent important determinants of susceptibility to related platinum drugs.

Additionally, our data suggest that a “translation addiction” in colorectal cancer is responsible for the effectiveness of oxaliplatin. Notably, other studies have indirectly associated the translation machinery with the mechanism of oxaliplatin-mediated cell

killing. In one study, three oxaliplatin resistant sublines were generated and microarrays were performed to compare the resistant and parental cell lines[50]. In each pair of cell lines, a significant portion of the differentially expressed transcripts between the resistant and parental lines corresponded to genes composing the ribosome. Another study generated an oxaliplatin sensitivity predictor based on NCI-60 oxaliplatin dose responses and cell line gene expression data[51], which enabled prediction of the responses to oxaliplatin in both cell lines *in vitro* as well as with patient colorectal cancer xenografts. Additionally, others used microarray technology to build gene expression signatures to that best predicted outcomes in clinical colorectal cancer cases. Despite this unbiased approach their signatures consisted of ribosome components[52–57]. Despite the implications for a role of the translation machinery in colorectal cancer, none of the aforementioned studies made such a connection.

mTOR-dependent translation elongation plays a critical role in colorectal cancer tumorigenesis[36]. For example, APC-deficient lesions increase protein synthesis, such that the progression of tumorigenesis is prevented by rapamycin. Thus, “translation addiction” accompanies colorectal cancer progression, making rapamycin an attractive therapeutic option. Additionally, our data indicate that APC and the translation machinery are linked in other cancer types. However, despite numerous attempts, rapamycin has not attained a solid foothold in cancer treatment, owing in part to cell intrinsic resistance mechanisms such as compensatory upregulation of PI3K signaling[58] and the development of rapamycin insensitive mTOR mutations[59]. In cancer types for which rapamycin has failed in clinical trials, oxaliplatin may be viewed as a preferable choice for inhibition of translation. Moreover, given the role of tumor-intrinsic Wnt signaling in suppressing anti-tumor T-cell immune responses[60], therapies like oxaliplatin that are more effective in Wnt activated tumors present a potential alternative to immunotherapy.

Although previous studies have identified differences in cellular response between cisplatin and oxaliplatin, ours is the first to identify causal links between oxaliplatin, ribosome biogenesis stress and cell death. For instance, oxaliplatin creates fewer cross-links per base than cisplatin, yet retains its cytotoxicity[61]. We suggest that the ability of oxaliplatin to cross-link DNA may be of questionable relevance, for we do not see activation of the DNA damage response. However, oxaliplatin-modified DNA could still lead to inhibition of rRNA synthesis, which would ultimately be responsible for ribosome biogenesis stress. In addition, one can envision scenarios in which oxaliplatin-modified rRNA, mRNA and/or protein could all potentially contribute to ribosome biogenesis stress. A DNA damage response-independent mechanism of cell death is consistent with previous observations that cisplatin- or oxaliplatin-resistant cell lines often do not exhibit cross-resistance[3]. Finally, an analysis of the effects of various chemotherapeutics at a range of concentrations on rRNA synthesis and processing found that at high enough concentrations of many agents, including cisplatin and oxaliplatin, perturb this process[62]. However, this study did not ascribe a causal link between ribosome biogenesis perturbation and cell death. Thus, although many chemotherapeutics may inhibit ribosome biogenesis at high drug concentrations, this behavior is unlikely to be their primary mechanism of action. Our findings demonstrate that at clinically relevant, and lower, concentrations oxaliplatin causes ribosome biogenesis stress whereas cisplatin does not. Thus, our work demonstrates that perturbation of ribosome biogenesis is functionally important for oxaliplatin, and not cisplatin, to mediate cell death.

Online Methods

shRNA Constructs

All shRNAs used were in the MLS retroviral vector with the exception of RPL11 in TMPVIR[63,64]. Transfection and infection were performed as previously described[6]. Unless shown, all knockdowns were previously validated for knockdown and off-target effects[5]. shRNA target sequences listed in Supplementary Table S9.

GFP Competition Assays

Eμ-Myc$^{p19arf-/-}$, *Eμ-Myc*$^{p53-/-}$ lymphoma or p185+ *BCR-Abl*$^{p19arf-/-}$ leukemia cells were infected with GFP-tagged shRNAs such that 15–25% of the population were GFP positive. An eighth of a million cells in 250μL B-cell media (BCM) were then seeded into 24-well plates. For wells that would remain untreated as a control, only 1/16th of a million cells were seeded. Next, 250μL of drug containing media was added to the cells. After 24 h, 300μL of cells from untreated wells are removed and replaced by 300μL fresh BCM. All wells then received 500μL BCM before being placed in the incubator for another 24 hours. At 48 h, cells transduced with the control vector, MLS, were checked for viability via flow cytometry on a BD FACScan using propidium iodide (PI) as a live/dead marker. Untreated wells then had 700μL of cells removed and replaced with 700μL fresh media followed by a further 1mL of fresh media. Wells for which drug had killed 80–90% of cells (LD80–90) were then diluted further by adding 1mL of BCM. Finally, at 72 h all wells for which an LD80–90 was achieved, as well as the untreated samples, were run via flow cytometry to determine GFP%. For shRPL11 experiments the above procedures were followed except in the presence of 1μg/mL doxycycline, including 24 h of pre-incubation of the hairpin containing cells in doxycycline. For all competition assays, at least three separate biological replicates were performed. Here, we define biological replicates as a fresh thaw that was infected, selected or sorted if necessary, then run through the comeptition assay.

RNAi Signatures

Drugs were dosed to achieve an LD80–90 in *Eμ-Myc p19*$^{arf-/-}$ cells by propidium iodide exclusion as determined by flow cytometry at 48 h. GFP enrichment/depletion was then determined by flow cytometry at 72 h. Linkage ratios and *p*-values were generated as described previously[5–7]. All flow cytometry was conducted using a BD FACScan. For all RNA signatures, at least three separate biological replicates were performed. Here, we define biological replicates as a fresh thaw of *Eμ-Myc p19*$^{arf-/-}$ cells that were infected, selected or sorted if necessary, then run through the signature assay.

Code Availability

Parameters and code for the modified K nearest neighbors (K-NN) algorithm for determining drug mechanism of action can be found in previous publications[5,7].

Drug Doses

Unless otherwise noted, all drugs were administered to *Eμ-Myc*$^{p19arf-/-}$, *Eμ-Myc*$^{p53-/-}$ lymphoma or p185+ *BCR-Abl*$^{p19arf-/-}$ leukemia cells at a concentration to achieve an

LD80–90 and 48 h as assessed via flow cytometry on a BD FACScan using propidium iodide as a live/dead marker. For time-point experiments, a portion of each sample was cultured until 48 h post-treatment to assure LD80–90 was achieved. If not, that sample was discarded and not included in further analysis. Similarly rigorous equipotent dosing was followed for adherent cell lines by first dosing over a large concentration range for 96 h and analyzing cell number via CellTiter-Glo (Promega). Then, for future equipotent doses only concentrations that achieved an IC80 at 96 h were used. For area under the curve calculations, whole dose response curves were analyzed with at 96 h and analyzed via MatLab 2015a (MathWorks). All drug doses were performed in at least once from three independent cultures.

Cell Cycle

One to two million cells were collected per sample after treatment with a concentration of drug required to achieve an LD80–90 at 48 h for *Eμ-Myc*$^{p19arf-/-}$ or IC80 at 96 h for A549 and LoVo. They were washed in PBS and then resuspended in 1mL of PBS+2% fetal bovine serum (FBS). Cells were then fixed in 70% ethanol overnight at -20° C. Cells were then rehydrated with 5mL of PBS, spun out of ethanol and then washed in PBS. Next, 1mL of PI staining solution (3.8mM sodium citrate, 50μg/mL PI in PBS) and 20 μL of RNAse A were used to resuspend the pellet. Cells were then incubated overnight at 4°C before FACS on a BD FACScan. Cell cycle profiles were analyzed using FlowJo V10.

RNA Isolation and Expression Analysis

Total RNA was isolated via QIAshredder and Qiagen RNeasy Mini Kit and cDNA was generated via M-MLV Reverse Transcriptase with RNaseOUT (ThermoFisher Scientific) and random hexamers. qRT-PCR was performed with Fast SYBER Green Mastermix and StepOnePlus Real-Time PCR System (Applied Biosystems) with three biological replicates, each with two technical replicates. Primer sequences listed in Supplementary Table S10.

Western Blotting

Cell pellets were washed in PBS and frozen before being lysed in RIPA buffer. They were then boiled after the addition of Laemmli sample buffer and run on an SDS-PAGE gel. From the gel they were transferred to Millipore immobilin-P membranes. The antibodies used were mouse anti-p53 (NCL-p53–505, Novocastra; 1:500), human anti-p53 (2524, Cell Signaling; 1:1,000), anti-phospho p53 (Ser 15) (9284, Cell Signaling; 1:1,000), anti-phospho p53 (Ser 20) (9287, Cell Signaling; 1:1,000), anti-γ-H2AX (20E3, Cell Signaling; 1:1,000), anti-p21 (sc-6246, Santa Cruz, 1:200), anti-cPARP1 (9544, Cell Signaling, 1:1,000), anti-GAPDH (sc-32233, Santa Cruz, 1:200), anti-β-actin (13E5, Cell Signaling; 1:1,000), anti-HSP90 (68/Hsp90, Becton Dickinson; 1:6,000).

Cell Culture

Eμ-Myc p19$^{arf-/-}$, *Eμ-Myc p53*$^{-/-}$ and p185+ *BCR-Abl p19*$^{arf-/-}$ primary murine tumor cells were cultured according to established protocols[65]. DT40 cells were cultured at 37°C with 5% CO2 in RPMI-1640 medium with glutamine (11875, Invitrogen, Carlsbad, CA) supplemented with 1% chicken serum (16110-082, Invitrogen, Carlsbad, CA), 10-5 M β-

mercaptoethanol (M-3148, Sigma-Aldrich, St. Louis, MO), penicillin-streptomycin (15140-122, Invitrogen), and 10% FBS (100-106, Gemini Bio-Products, West Sacramento, CA). A549, SW480, LoVo, CAMA-1, Hs578T, ZR-75-1, BT549, SK-BR-3 and HCC1937 cells were obtained from ATCC (CCL-185, CCL-228, CCL-229, HTB-21, HTB-126, CRL-1500, HTB-122, HTB-30 and CRL-2336) and cultured according to ATCC guidelines. All cell lines, except those obtained and used directly from ATCC, were tested for mycoplasma and found to be negative (MycoAlert, Lonza). No authentication was performed.

Cellular Uptake of Platinum

Two million *Eμ-Myc p19*$^{arf-/-}$ cells were dosed at concentrations required to achieve an LD80–90 at 48 h or at 5μM in three biological replicates. After 3 h, they were washed three times in PBS, pelleted and frozen. Atomic absorption spectroscopic analysis was then performed as previously described[66].

Structure-based Hierarchical Clustering

The ChemmineR R package was used to calculate Tanimoto coefficients and perform hierarchical clustering.

DT40 Knockout Line Drug Sensitivity Analysis

To measure the sensitivity, cells were continuously exposed to various concentrations of drugs for 72 h in triplicate. Cell survival was determined using the ATPlite 1-step kit (PerkinElmer) and an EnVision 2104 Multilabel Reader. To evaluate the relative cellular sensitivity of each mutant to wild type cells, logarithm sensitivity curves were used to determine the concentration that causes 90% reduction of ATP activity (IC_{90}). The IC_{90} value of each mutant was divided by that of wild type cells on the same plate. Finally, the quotient was converted to a logarithmic scale (base 2). Pairwise distances were calculated via the ‘pdist’ function with the Euclidian distance metric in Matlab 2013b.

Immunofluorescence Staining

Eμ-Myc p19$^{arf-/-}$ cells were dosed at an LD80–90 and after 4 or 8 h of treatment placed on slides via cytospin. LoVo cells were dosed at IC_{80} and fixed after 12 h or treatment. Cells were then dried and stained with anti-γ-H2AX (20E3, Cell Signaling; 1:500) and DAPI or anti-NPM (B0556, Sigma, 1:2000), anti-Fibrillarin (ab5821, Abcam, 1:500) and DAPI. Alex Fluor 488 or 555 was used as a secondary and then samples were mounted with Prolong Gold. An EVOS FL Auto microscope was used for imaging. Image analysis was performed using CellProfiler on the original images.

Comet Assays

Eμ-Myc p19$^{arf-/-}$ cells were dosed at an LD80–90 and after 6 h were washed and prepared for either alkaline or neutral comet assays. Comet tail analysis was performed using CaspLab using images that were all equally level adjusted in Adobe Photoshop. ZR-75-1 cells were dosed at an IC_{80} and after 24 h were washed and prepared for neutral comet

assays. CellProfiler was used to analyze ZR-75-1 comets. The Trevigen CometAssay Kit was used for both cell lines.

In vivo Competition Assay

Two million *Eμ-Myc p19*$^{arf-/-}$ cells were partially infected with shChk2 and tail vein injected into 8-week old female C57BL/6 mice. Cisplatin, oxaliplatin or phenanthriplatin in sterile saline were administered via intraperitoneal injection at disease presentation (7mg/kg, 5mg/kg or 3mg/kg, respectively) and mice were sacrificed and tumors harvested upon relapse, 2–3 days after treatment. Disease presentation and relapse were defined as the presence of palpable lymph node burden. Fold change in GFP% was assessed relative to untreated mice after tumor cell harvesting by flow cytometry on a BD FACScan. Each treatment group had five or six mice. This was chosen independently of statistical power analysis. No randomization or blinding methods were used to determine treatment branches. The experiment was performed in accordance to MIT's Committee on Animal Care (CAC) prior to execution.

Combination Doses and Bliss Independence

Eμ-Myc$^{p19arf-/-}$ lymphoma cells were treated with drug and analyzed as detailed above, except with two drugs in combination in a 3×5 dose response matrix where the outer wells were only exposed to a single drug[6]. The single drug wells were then used to calculate the expected Bliss Independence values of the combination wells. The expected Bliss Independence values were then subtracted from the observed values. The minimum or maximum value in the matrix was then chosen as the minimum or maximum percent excess under Bliss Independence.

Statistical Analysis

Two-sided, non-parametric tests were performed unless otherwise specified. If two conditions were compared, Mann-Whitney U-test was used. If more than one condition was compared to a control condition then one-way ANOVA with Dunnett's Multiple Comparison Test was used. If a t-test was used, the data were first confirmed to fit a normal distribution via the 'kstest' function in Matlab 2015a. See figure legends for details on type of replicate and n values used.

Principal Component Analysis

Principal component analysis (PCA) was used to provide another means of visualizing our data, and was not used to classify new compounds. This was done via Matlab 2015a. The 'pca' function was used with data from Supplementary Table S4 to generate the necessary input variables for the 'biplot' function.

Bioinformatic Analysis

CellMiner was used to obtain NCI-60 oxaliplatin sensitivity-expression level correlation values[30]. Benjamini-Hochberg correction was then used to eliminate genes above an FDR threshold of 0.05. For the TCGA tumor expression analysis, RNA-seq gene-level raw count data for colorectal and ovarian cancer tumor samples that went through the same pipeline for

generation of expression levels (RPKM values)(193 and 420 samples respectively) were downloaded from the TCGA data portal. The Bioconductor edgeR package in R was used to perform normalization and analysis for differential expression between these two cancer types[67]. We obtained 3247 significantly differentially expressed genes between these two cancer types, with a $\log_2$-fold change in normalized tag counts greater than 2.5 (corresponding to a Benjamini-Hochberg corrected p-value of 5.8E-3 from a negative binomial generalized linear model fit). Among these genes, 1909 and 1338 were significantly up-regulated and down-regulated, respectively, in ovarian cancer compared to colorectal cancer. Significantly correlated (NCI-60) or differentially expressed (TCGA) genes were then loaded in Gene Set Enrichment Analysis and the pre-ranked list tool was used[33].

For both NCI-60 and TCGA datasets a translation metagene was obtained by averaging expression of 120 genes known to be involved in translation for each. To demonstrate correlation between oxaliplatin sensitivity and translation, we plotted the GI50 values (log-scale) against the metagene expression levels for lung and breast cancer cell lines in the NCI-60 catalogue. To examine associations between Wnt pathway activity and expression levels of the translation machinery, we calculated Pearson correlation coefficients of the translation metagene expression with that of known Wnt pathway genes in the Reactome database for breast cancer samples in the TCGA database. A heatmap of expression values of translation machinery genes ordered by decreasing APC expression values was then plotted to visualize such correlations.

Ribosome Profiling

One million cells for each of three replicates were harvested by centrifugation at 300g for 5 m, resuspended in ice-cold PBS containing 100μg/mL cycloheximide and centrifuged again. Cell pellets were flash frozen in liquid nitrogen. To prepare the lysate, cell pellets were thawed in lysis buffer (10mM Tris-HCl, pH 7.4, 5mM MgCl2, 1% Triton X-100, 100mM KCl, 0.02U/μL Superase-IN, 2mM DTT, and 100μg/mL cycloheximide), passed four times through a 26-gauge needle and cleared by centrifugation at 1,300g for 10 m at 4°C. The supernatant was loaded onto a 10–50% w/v linear sucrose gradient containing 20mM HEPES-KOH, pH 7.4, 5mM MgCl2, 100mM KCl, 2mM DTT, 100μg/mL cycloheximide, and 0.02U/μL Superase-IN. Gradients were centrifuged for 2 h at 36,000 rpm and 4°C and then fractionated by upward displacement using a Biocomp Gradient Station with continuous absorbance monitoring at 254 nm. Traces were quantified using Fiji. Dosing of replicates was performed as technical replicates from the same culture that had been split into three the previous day. Profiling was conducted in two separate rounds, one set of samples together and the other two together in consecutive weeks.

Supplementary Material

Refer to Web version on PubMed Central for supplementary material.

Acknowledgments

This work was supported by National Cancer Institute Grant CA034992 (S.J.L.) and a Misrock Postdoctoral Fellowship (G.Y.P.). M.T.H. is the Chang and Eisen Associate Professor of Biology. Funding was provided by ICBP #U54-CA112967-09. C.E.K. was supported by award Number T32GM007753 from the National Institute of General Medical Sciences. Our studies are supported by the Center of Cancer Research, the Intramural Program of the National Cancer Institute, NIH (Z01 BC006150-19). This work was also supported in part by the Koch Institute Support (core) Grant P30-CA14051 from the National Cancer Institute. We thank J. Wilson for providing platinum compounds ([Pt(tfbz)$(NH_3)_2$](NO_3) and [Pt(acac)$(NH_3)_2$]$(SO_4)_{0.5}$) and D. Bartel for advice and discussion regarding translation and ribosome translation experiments. The authors also thank G. Walker, A. Koehler, E. Bent, C. Braun, E. Kreidl, and B. Zhao for comments and discussion on the paper and N. Fenouille, H. Criscione, and F. Lam for technical assistance. Also, we acknowledge G. Paradis and the Koch Institute Flow Cytometry Facility for advice and services. The content is solely the responsibility of the authors and does not necessarily represent the official views of the National Institute of General Medical Sciences or the National Institutes of Health.

References

1. Kelland L. The resurgence of platinum-based cancer chemotherapy. Nat Rev Cancer. 2007; 7:573–584. [PubMed: 17625587]
2. DeVita, VT., Chu, E., Chu, Edward, DeVita, VT, Jr. Cancer research. Vol. 68. Jones & Bartlett Learning Oncology; 2008. Physician's Cancer Chemotherapy Drug Manual.
3. Rixe O, et al. Oxaliplatin, tetraplatin, cisplatin, and carboplatin: spectrum of activity in drug-resistant cell lines and in the cell lines of the National Cancer Institute's Anticancer Drug Screen panel. Biochem Pharmacol. 1996; 52:1855–65. [PubMed: 8951344]
4. Machover D, et al. Two consecutive phase II studies of oxaliplatin (L-OHP) for treatment of patients with advanced colorectal carcinoma who were resistant to previous treatment with fluoropyrimidines. Ann Oncol Off J Eur Soc Med Oncol. 1996; 7:95–8.
5. Jiang H, Pritchard JR, Williams RT, Lauffenburger DA, Hemann MT. A mammalian functional-genetic approach to characterizing cancer therapeutics. Nat Chem Biol. 2011; 7:92–100. [PubMed: 21186347]
6. Pritchard JR, et al. Defining principles of combination drug mechanisms of action. Proc Natl Acad Sci U S A. 2013; 110:E170–9. [PubMed: 23251029]
7. Pritchard JR, Bruno PM, Hemann MT, Lauffenburger DA. Predicting cancer drug mechanisms of action using molecular network signatures. Mol Biosyst. 2013; 9:1604–19. [PubMed: 23287973]
8. Suntharalingam K, et al. Bidentate Ligands on Osmium(VI) Nitrido Complexes Control Intracellular Targeting and Cell Death Pathways. J Am Chem Soc. 2013; 135:14060–14063. [PubMed: 24041161]
9. Suntharalingam K, et al. A Breast Cancer Stem Cell Selective, Mammospheres Potent Osmium(VI) Nitrido Complex. J Am Chem Soc. 2014; 136:14413–14416. [PubMed: 25247635]
10. Suntharalingam K, et al. Necroptosis-Inducing Rhenium(V) Oxo Complexes. J Am Chem Soc. 2015; 137:2967–2974. [PubMed: 25698398]
11. Awuah SG, Zheng YR, Bruno PM, Hemann MT, Lippard SJA. Pt(IV) Pro-drug Preferentially Targets Indoleamine-2,3-dioxygenase, Providing Enhanced Ovarian Cancer Immuno-Chemotherapy. J Am Chem Soc. 2015; :jacs.5b10182.doi: 10.1021/jacs.5b10182
12. Boodram JN, et al. Breast Cancer Stem Cell Potent Copper(II)-Non-Steroidal Anti-Inflammatory Drug Complexes. Angew Chemie Int Ed. 2016; 55:2845–2850.
13. Cressey PB, et al. The Potent Inhibitory Effect of a Naproxen-Appended Cobalt(III)-Cyclam Complex on Cancer Stem Cells. ChemBioChem. 2016; 17:1713–1718. [PubMed: 27377813]
14. Zheng YR, et al. Mechanistic studies of the anticancer activity of an octahedral hexanuclear Pt(II) cage. Inorganica Chim Acta. 2016; 452:125–129. [PubMed: 27818526]
15. Barnes JC, et al. Using an RNAi Signature Assay To Guide the Design of Three-Drug-Conjugated Nanoparticles with Validated Mechanisms, In Vivo Efficacy, and Low Toxicity. J Am Chem Soc. 2016; :jacs.6b06321.doi: 10.1021/jacs.6b06321
16. Zamble DB, Mu D, Reardon JT, Sancar A, Lippard SJ. Repair of cisplatin–DNA adducts by the mammalian excision nuclease. Biochemistry. 1996; 35:10004–13. [PubMed: 8756462]

17. Fojo T, et al. Identification of non-cross-resistant platinum compounds with novel cytotoxicity profiles using the NCI anticancer drug screen and clustered image map visualizations. Crit Rev Oncol Hematol. 2005; 53:25–34. [PubMed: 15607933]
18. Alvarez M, et al. Generation of a drug resistance profile by quantitation of mdr-1/P-glycoprotein in the cell lines of the National Cancer Institute Anticancer Drug Screen. J Clin Invest. 1995; 95:2205–14. [PubMed: 7738186]
19. Willett P, Barnard JM, Downs GM. Chemical Similarity Searching. J Chem Inf Model. 1998; 38:983–996.
20. Williams RT, Roussel MF, Sherr CJ. Arf gene loss enhances oncogenicity and limits imatinib response in mouse models of Bcr-Abl-induced acute lymphoblastic leukemia. Proc Natl Acad Sci U S A. 2006; 103:6688–93. [PubMed: 16618932]
21. Winding P, Berchtold MW. The chicken B cell line DT40: a novel tool for gene disruption experiments. J Immunol Methods. 2001; 249:1–16. [PubMed: 11226459]
22. Jiang H, et al. The combined status of ATM and p53 link tumor development with therapeutic response. Genes Dev. 2009; 23:1895–1909. [PubMed: 19608766]
23. Rogakou EP, Nieves-Neira W, Boon C, Pommier Y, Bonner WM. Initiation of DNA fragmentation during apoptosis induces phosphorylation of H2AX histone at serine 139. J Biol Chem. 2000; 275:9390–9395. [PubMed: 10734083]
24. Bonner WM, et al. γH2AX and cancer. Nat Rev Cancer. 2008; 8:957–967. [PubMed: 19005492]
25. Olive PL, Banáth JP. The comet assay: a method to measure DNA damage in individual cells. Nat Protoc. 2006; 1:23–9. [PubMed: 17406208]
26. Golomb L, Volarevic S, Oren M. P53 and ribosome biogenesis stress: The essentials. FEBS Lett. 2014; 588:2571–2579. [PubMed: 24747423]
27. Boulon S, Westman BJ, Hutten S, Boisvert FM, Lamond AI. The Nucleolus under Stress. Mol Cell. 2010; 40:216–227. [PubMed: 20965417]
28. Liu J, Xu Y, Stoleru D, Salic a. Imaging protein synthesis in cells and tissues with an alkyne analog of puromycin. Proc Natl Acad Sci. 2012; 109:413–418. [PubMed: 22160674]
29. Bliss CI. The calculation of microbial assays. Bacteriol Rev. 1956; 20:243–58. [PubMed: 13403845]
30. Reinhold WC, et al. CellMiner: a web-based suite of genomic and pharmacologic tools to explore transcript and drug patterns in the NCI-60 cell line set. Cancer Res. 2012; 72:3499–511. [PubMed: 22802077]
31. Huang DW, Sherman BT, Lempicki Ra. Bioinformatics enrichment tools: Paths toward the comprehensive functional analysis of large gene lists. Nucleic Acids Res. 2009; 37:1–13. [PubMed: 19033363]
32. Huang DW, Sherman BT, Lempicki Ra. Systematic and integrative analysis of large gene lists using DAVID bioinformatics resources. Nat Protoc. 2009; 4:44–57. [PubMed: 19131956]
33. Subramanian A, et al. Gene set enrichment analysis: a knowledge-based approach for interpreting genome-wide expression profiles. Proc Natl Acad Sci U S A. 2005; 102:15545–50. [PubMed: 16199517]
34. Cancer Genome Atlas Research Network. Integrated genomic analyses of ovarian carcinoma. Nature. 2011; 474:609–615. [PubMed: 21720365]
35. Muzny DM, et al. Comprehensive molecular characterization of human colon and rectal cancer. Nature. 2012; 487:330–337. [PubMed: 22810696]
36. Faller WJ, et al. mTORC1-mediated translational elongation limits intestinal tumour initiation and growth. Nature. 2014; 517:497–500. [PubMed: 25383520]
37. Koboldt DC, et al. Comprehensive molecular portraits of human breast tumours. Nature. 2012; 490:61–70. [PubMed: 23000897]
38. Raymond E, Chaney SG, Taamma A, Cvitkovic E. Oxaliplatin: a review of preclinical and clinical studies. Ann Oncol. 1998; 9:1053–71. [PubMed: 9834817]
39. Raymond E, Lawrence R, Izbicka E, Faivre S, Von Hoff DD. Activity of oxaliplatin against human tumor colony-forming units. Clin Cancer Res. 1998; 4:1021–9. [PubMed: 9563898]

40. Shelley MD, Burgon K, Mason MD. Treatment of testicular germ-cell cancer: a cochrane evidence-based systematic review. Cancer Treat Rev. 2002; 28:237–53. [PubMed: 12435371]
41. Goldberg RM, et al. A randomized controlled trial of fluorouracil plus leucovorin, irinotecan, and oxaliplatin combinations in patients with previously untreated metastatic colorectal cancer. J Clin Oncol. 2004; 22:23–30. [PubMed: 14665611]
42. Raez LE, et al. Efficacy and safety of oxaliplatin and docetaxel in patients with locally advanced and metastatic non-small-cell lung cancer (NSCLC). Lung Cancer. 2006; 53:347–53. [PubMed: 16844257]
43. Atmaca A, et al. A randomised multicentre phase II study with cisplatin/docetaxel vs oxaliplatin/docetaxel as first-line therapy in patients with advanced or metastatic non-small cell lung cancer. Br J Cancer. 2013; :1–6. DOI: 10.1038/bjc.2012.555
44. Scagliotti GV, et al. Pemetrexed combined with oxaliplatin or carboplatin as first-line treatment in advanced non-small cell lung cancer: a multicenter, randomized, phase II trial. Clin Cancer Res. 2005; 11:690–6. [PubMed: 15701857]
45. Yardley DA, et al. A phase II trial of oxaliplatin and trastuzumab in the treatment of HER2-positive metastatic breast cancer. Cancer investigation. 2010; 28
46. Njiaju UO, et al. Capecitabine and oxaliplatin in combination as first- or second-line therapy for metastatic breast cancer: A Wisconsin Oncology Network trial. Cancer Chemother Pharmacol. 2013; 71:613–618. [PubMed: 23228989]
47. Guerrero A, et al. Phase I/II study of biweekly vinorelbine and oxaliplatin as first-line treatment in patients with metastatic breast cancer. Anticancer Drugs. 2011; 22:283–289. [PubMed: 21150776]
48. Imielinski M, et al. Mapping the hallmarks of lung adenocarcinoma with massively parallel sequencing. Cell. 2012; 150:1107–20. [PubMed: 22980975]
49. Meijers-Heijboer H, et al. Low-penetrance susceptibility to breast cancer due to CHEK2(*)1100delC in noncarriers of BRCA1 or BRCA2 mutations. Nat Genet. 2002; 31:55–9. [PubMed: 11967536]
50. Samimi G, et al. cDNA microarray-based identification of genes and pathways associated with oxaliplatin resistance. Cancer Chemother Pharmacol. 2005; 55:1–11. [PubMed: 15378272]
51. Kim MK, et al. Characterization of an oxaliplatin sensitivity predictor in a preclinical murine model of colorectal cancer. Mol Cancer Ther. 2012; 11:1500–9. [PubMed: 22351745]
52. Bertucci F, et al. Gene expression profiling of colon cancer by DNA microarrays and correlation with histoclinical parameters. Oncogene. 2004; 23:1377–1391. [PubMed: 14973550]
53. Arango D, et al. Gene-expression profiling predicts recurrence in Dukes' C colorectal cancer. Gastroenterology. 2005; 129:874–884. [PubMed: 16143127]
54. Barrier A, et al. Stage II colon cancer prognosis prediction by tumor gene expression profiling. J Clin Oncol. 2006; 24:4685–4691. [PubMed: 16966692]
55. Yamasaki M, et al. The gene expression profile represents the molecular nature of liver metastasis in colorectal cancer. Int J Oncol. 2007; 30:129–138. [PubMed: 17143521]
56. Bandrés E, et al. A gene signature of 8 genes could identify the risk of recurrence and progression in Dukes' B colon cancer patients. Oncol Rep. 2007; 17:1089–1094. [PubMed: 17390049]
57. Fritzmann J, et al. A colorectal cancer expression profile that includes transforming growth factor beta inhibitor BAMBI predicts metastatic potential. Gastroenterology. 2009; 137:165–75. [PubMed: 19328798]
58. Zoncu R, Efeyan A, Sabatini D. M mTOR: from growth signal integration to cancer, diabetes and ageing. Nat Rev Mol Cell Biol. 2011; 12:21–35. [PubMed: 21157483]
59. Voss MH, et al. Tumor genetic analyses of patients with metastatic renal cell carcinoma and extended benefit from mTOR inhibitor therapy. Clin Cancer Res. 2014; 20:1955–64. [PubMed: 24622468]
60. Spranger S, Bao R, Gajewski TF. Melanoma-intrinsic β-catenin signalling prevents anti-tumour immunity. Nature. 2015; 523:231–235. [PubMed: 25970248]
61. Woynarowski JM, et al. Oxaliplatin-induced damage of cellular DNA. Mol Pharmacol. 2000; 58:920–7. [PubMed: 11040038]

62. Burger K, et al. Chemotherapeutic drugs inhibit ribosome biogenesis at various levels. J Biol Chem. 2010; 285:12416–25. [PubMed: 20159984]

63. Dickins, Ra, et al. Probing tumor phenotypes using stable and regulated synthetic microRNA precursors. Nat Genet. 2005; 37:1289–95. [PubMed: 16200064]

64. Zuber J, et al. Toolkit for evaluating genes required for proliferation and survival using tetracycline-regulated RNAi. Nat Biotechnol. 2011; 29:79–83. [PubMed: 21131983]

65. Zhao B, Pritchard JR, Lauffenburger DA, Hemann MT. Addressing Genetic Tumor Heterogeneity through Computationally Predictive Combination Therapy. Cancer Discov. 2014; 4:166–74. [PubMed: 24318931]

66. Park GY, Wilson JJ, Song Y, Lippard SJ. Phenanthriplatin, a monofunctional DNA-binding platinum anticancer drug candidate with unusual potency and cellular activity profile. Proc Natl Acad Sci U S A. 2012; 109:11987–92. [PubMed: 22773807]

67. Robinson MD, McCarthy DJ, Smyth GK. edgeR: A Bioconductor package for differential expression analysis of digital gene expression data. Bioinformatics. 2009; 26:139–140. [PubMed: 19910308]

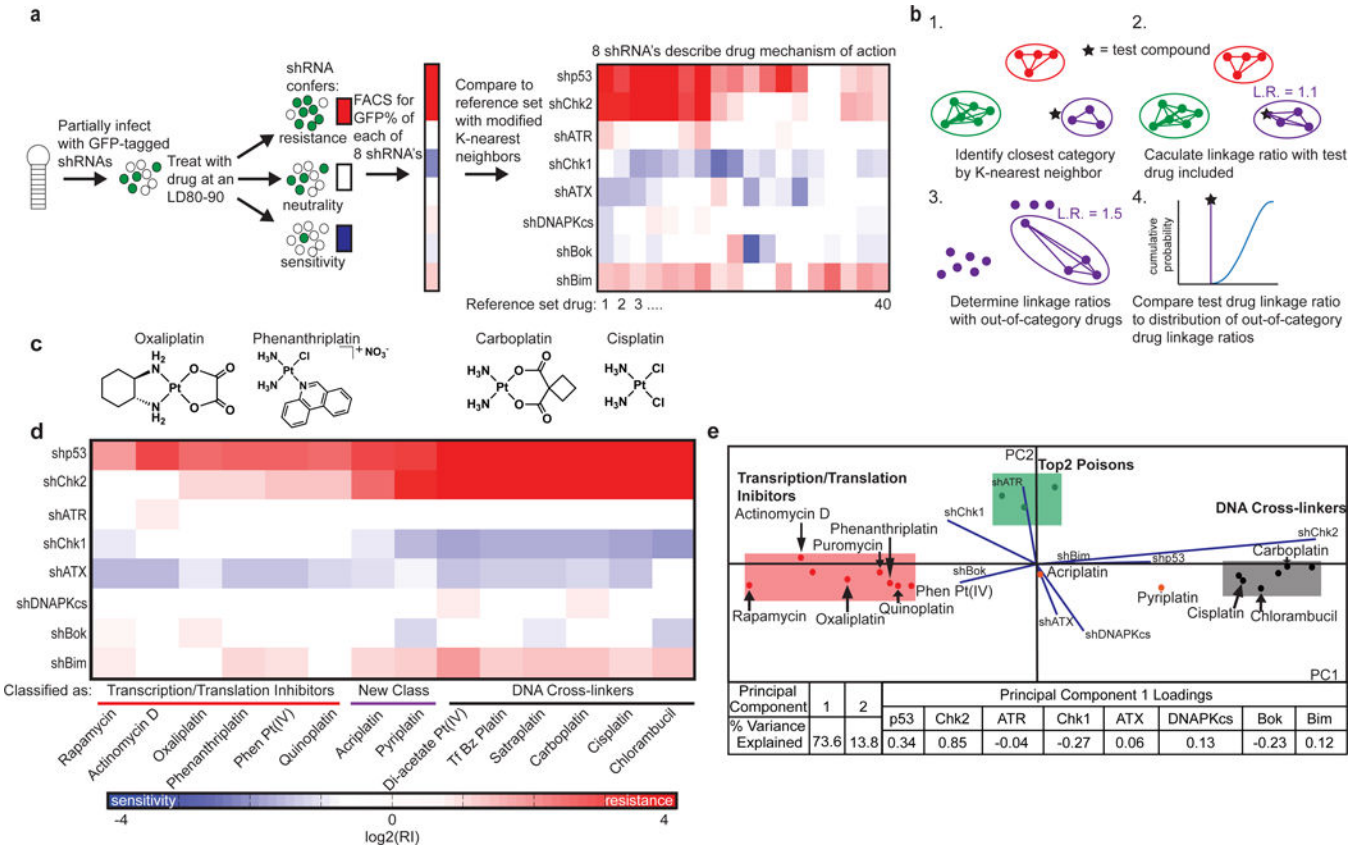

Principal Component	1	2	Principal Component 1 Loadings							
% Variance Explained	73.6	13.8	p53	Chk2	ATR	Chk1	ATX	DNAPKcs	Bok	Bim
			0.34	0.85	-0.04	-0.27	0.06	0.13	-0.23	0.12

Figure 1.

RNAi signatures identify a spectrum of platinum drug activities. (**a**) A schematic representation of our signature-based approach. *Eμ-Myc p19*$^{Arf-/-}$ lymphoma cells are partially infected with GFP-tagged shRNAs targeting the indicated eight genes. The individual pools of eight shRNA containing cells are treated with drug to achieve 80–90% killing at 48 h. Relative GFP% is measured at 72 h by flow cytometry and the subsequent shRNA signature is compared to our reference set using our modified K-nearest neighbors algorithm. (**b**) A schematic representation of our modified K-nearest neighbors algorithm. First, the test compound's nearest reference set category is identified by Euclidian K-nearest neighbor's analysis. Second, the linkage ratio (L.R.) is determined by dividing the pairwise distances of the category containing the new drug by the category without the new drug. Third, the linkage ratios are then calculated for all out-of-category drugs as if they were members of the category in question. This generates a background distribution of negative control linkage ratios. Fourth, the linkage ratio of the new drug is compared to the linkage ratio distribution of the negative controls to obtain a p-value. If $p > 0.05$ then drug is classified as belonging to a "new class" and having a mechanism of action not represented in the reference set. (**c**) On the right, cisplatin and carboplatin, two of the three clinically approved platinum agents classify as DNA cross-linkers. On the left, oxaliplatin, the third clinically approved platinum agent, and phenanthriplatin, a mono-functional platinum agent, both classify as transcription/translation inhibitors. (**d**) A heat map showing platinum compound signatures, with reference compounds rapamycin, actinomycin D and chlorambucil included. Rapamycin and actinomycin D represent transcription/translation

inhibitors whereas chlorambucil represents DNA cross-linkers. The other agents are shown classified according to their respective labels. (**e**) Principal components analysis of the platinum compounds Top2 poisons, DNA cross-linkers and transcription/translation inhibitors. Tables show the percent variance explained by each principal component, as well as the principal component 1 loadings depicting the percent contribution of each of the eight shRNAs for the PCA shown above. Shaded boxes represent the approximate space the category occupies in the PCA and are only meant to aid visualization, not category classification.

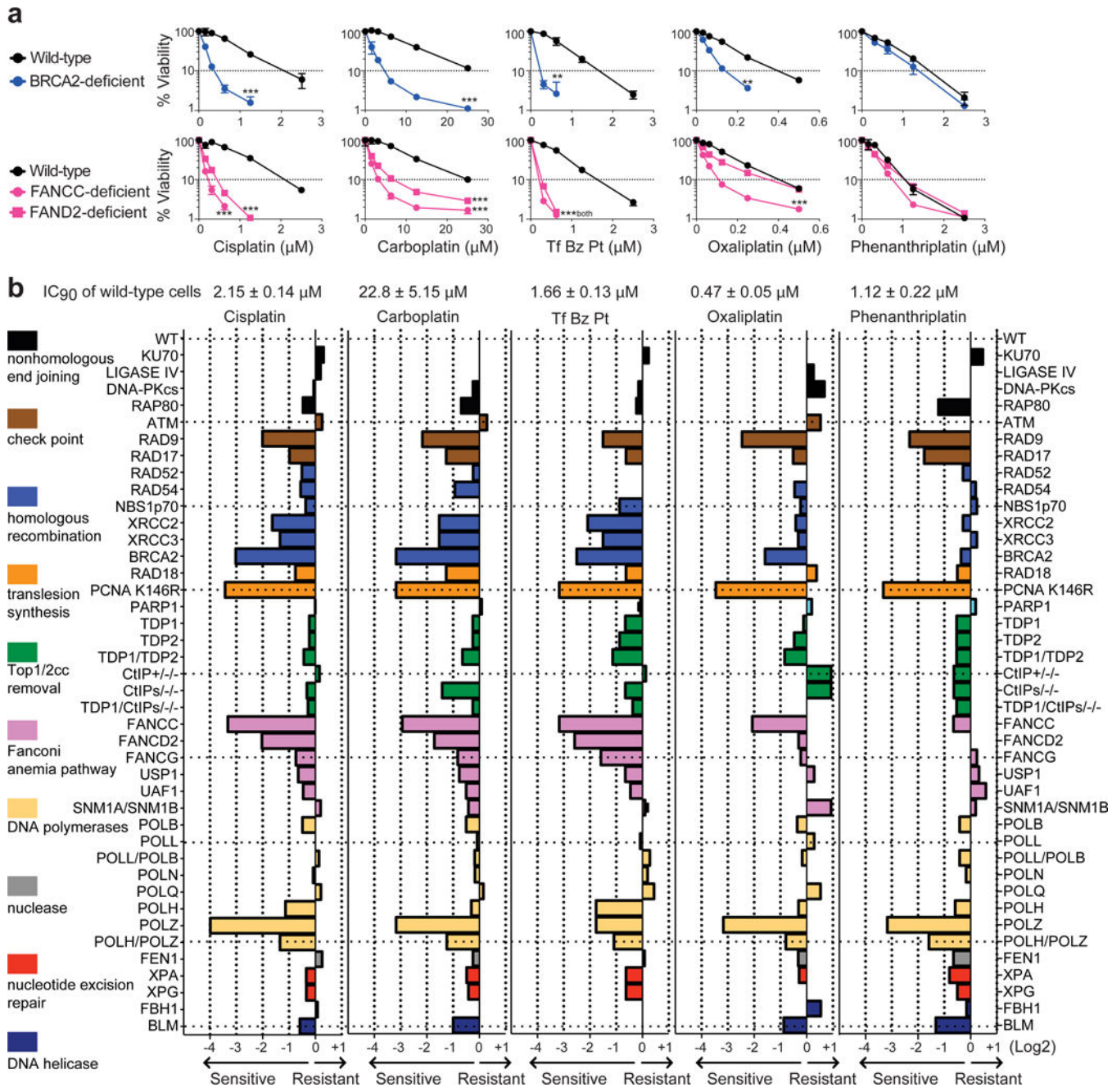

Figure 2.

Sensitivity profiles of the indicated platinum drugs on a panel of the repair-deficient DT40 mutants. (**a**) Viability curves of the indicated cell lines after continuous treatment for 72 h with the indicated drugs. Error bars represent the S.D. (n=3). $p < 0.05$ (*), $p < 0.01$ (**) or $p < 0.001$ (***) by unpaired two-tailed Student's t-test on the highest doses only. (**b**) Relative sensitivity of all of the DT40 mutant cell lines. A negative score and a positive score indicates that the cells are sensitive and resistant to the drug, respectively. The score is $\log_2$ of the difference between IC_{90} (inhibitory concentration 90%) values. IC_{90} of wild-type cells are shown at the top of each panel (n=8–10). n = 3 for all others. The bars are colored

according to the main DNA repair function of deficient gene(s). Black; nonhomologous end joining (NHEJ), brown; check point, blue; homologous recombination (HR), orange: translesion synthesis (TLS), aqua; PARP1, green; removal of topoisomerase I or topoisomerase II cleavage complex, pink; Fanconi anemia (FA) pathway, light orange; DNA polymerase, grey; nuclease, red; nucleotide excision repair (NER), dark blue; DNA helicase.

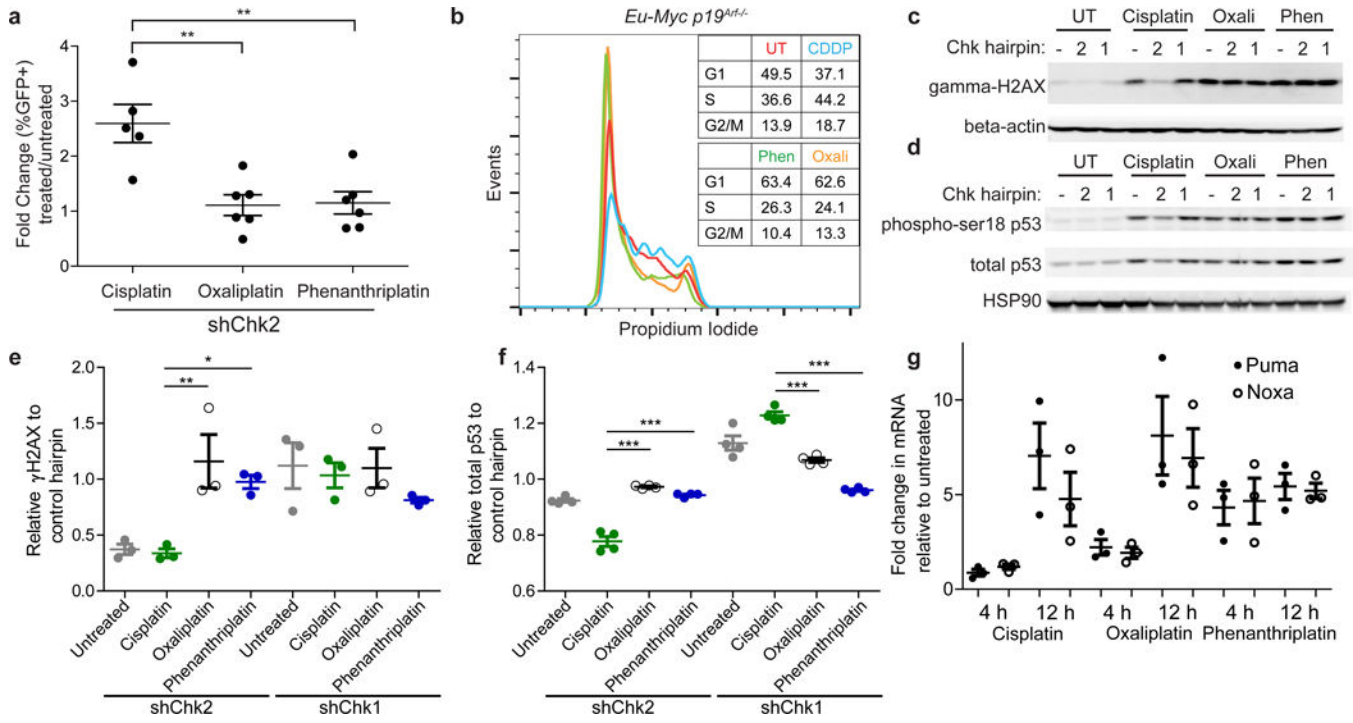

Figure 3.

Phenanthriplatin and oxaliplatin exhibit distinct differences from cisplatin in cell cycle profiles, γ-H2AX and p53 signaling in *Eμ-Myc p19*$^{arf-/-}$ cells. (**a**) Results of an *in vivo* GFP competition assay. Fold change in GFP% was assessed relative to untreated mice after tumor cell harvesting. $p < 0.01$ (**) by a two-tailed Mann-Whitney test. Mean ± SEM is depicted. n = 5 for all conditions. (**b**) Cell cycle profiles of resulting from 12 h treatment by cisplatin, phenanthriplatin or oxaliplatin. UT: Untreated, CDDP: cisplatin, Phen: phenanthriplatin, Oxali: oxaliplatin (**c**) Western blot for γ-H2AX after cisplatin, oxaliplatin or phenanthriplatin treatment with or without shChk2 or shChk1 at 12 h. (**d**) Western blot for phospho-ser18 and total p53 after cisplatin, oxaliplatin or phenanthriplatin treatment with or without shChk2 or shChk1 at 12 h. (e) Densitometry quantification of Fig. 3c. Data are mean ± SEM via three independent quantification results. $p < 0.05$ (*), $p < 0.01$ (**) for each group relative to cisplatin shChk2 or shChk1 by one-way ANOVA with Dunnett's Multiple Comparison Test. (**f**) Densitometry quantification of Fig. 3d. Data are mean ± SEM via four independent quantification results. $p < 0.001$ (***) for each group relative to cisplatin shChk2 or shChk1 by one-way ANOVA with Dunnett's Multiple Comparison Test. (**g**) Results of qPCR analysis conducted for Puma and Noxa after 4 and 12 h of cisplatin, phenanthriplatin or oxaliplatin treatment. Data are represented as mean ± SEM. n = 3 from independent experiments from independent cultures of cells.

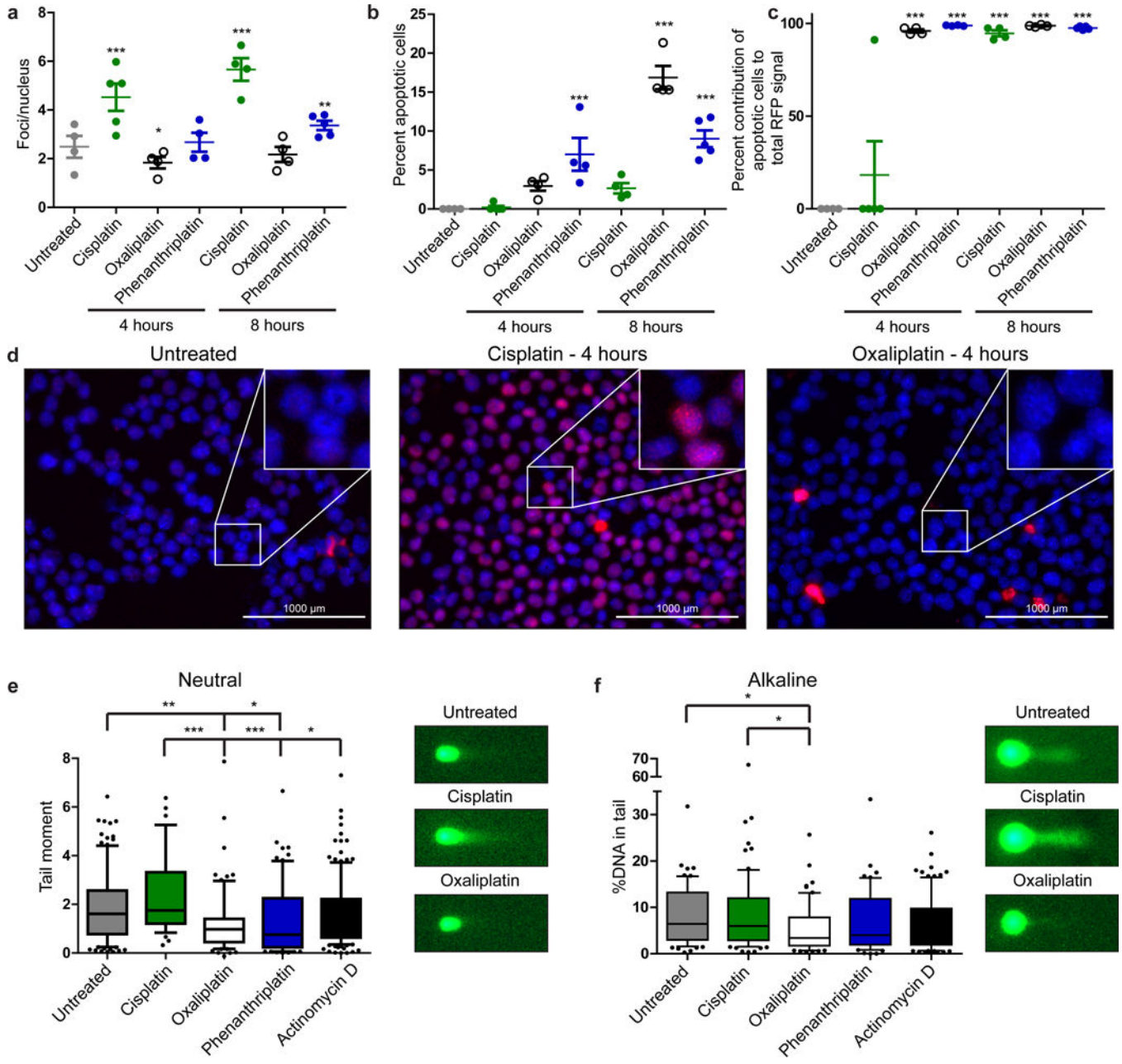

Figure 4.

Immunofluorescence of γ-H2AX and comet assays reveal lack of DNA damage resulting from oxaliplatin and phenanthriplatin treatment in *Eμ-Myc p19*$^{arf-/-}$ cells. (**a**) Foci per nucleus for each condition at both 4 h and 8 h after treatment. Data are represented as mean ± SEM for each field. $p < 0.05$ (*), $p < 0.01$ (**) or $p < 0.001$ (***) for each group relative to untreated by one-way ANOVA with Dunnett's Multiple Comparison Test. (**b**) Apoptotic cells identified via pan-nuclear γ-H2AX as a percent of total nuclei. Data are represented as mean ± SEM for each field. $p < 0.0005$ (***) for each group relative to untreated by one-way ANOVA with Dunnett's Multiple Comparison Test. (**c**) The sum of the integrated intensity of pan-nuclear γ-H2AX divided by the total RFP signal for each field. Data are represented

as mean ± SEM for each field. $p < 0.0005$ (***) for each group relative to untreated by one-way ANOVA with Dunnett's Multiple Comparison Test. For a-c, 4 fields were analyzed for each condition except 4 h cisplatin and 8 h phenanthriplatin which had 5 each. (**d**) Representative images of γ-H2AX immunofluorescence staining. Insets are 2.5× magnified. (**e**) Quantification of tail moment after performing a neutral comet assay 6 h after indicated drug treatment. Box center line represents the mean and box limits are quartiles 1 and 3, and whiskers show 10th and 90th percentile. On the right, representative images from each untreated, cisplatin and oxaliplatin treated cells. $p < 0.05$ (*), $p < 0.01$ (**) or $p < 0.001$ (***) for each group relative to untreated or cisplatin by one-way ANOVA with Dunnett's Multiple Comparison Test. Number of comets analyzed for untreated, cisplatin, oxaliplatin, phenanthriplatin and actinomycin D were 117, 37, 77, 76 and 143, respectively. (**f**) Quantification of percent DNA in tail after performing a neutral comet assay 6 h after indicated drug treatment. Box center line represents the mean and box limits are quartiles 1 and 3, and whiskers show 10th and 90th percentile. On right, representative images from each untreated, cisplatin and oxaliplatin treated cells. $p < 0.05$ (*) for each group relative to untreated or cisplatin by one-way ANOVA with Dunnett's Multiple Comparison Test. Number of comets analyzed for untreated, cisplatin, oxaliplatin, phenanthriplatin and actinomycin D were 67, 77, 64, 50 and 91, respectively.

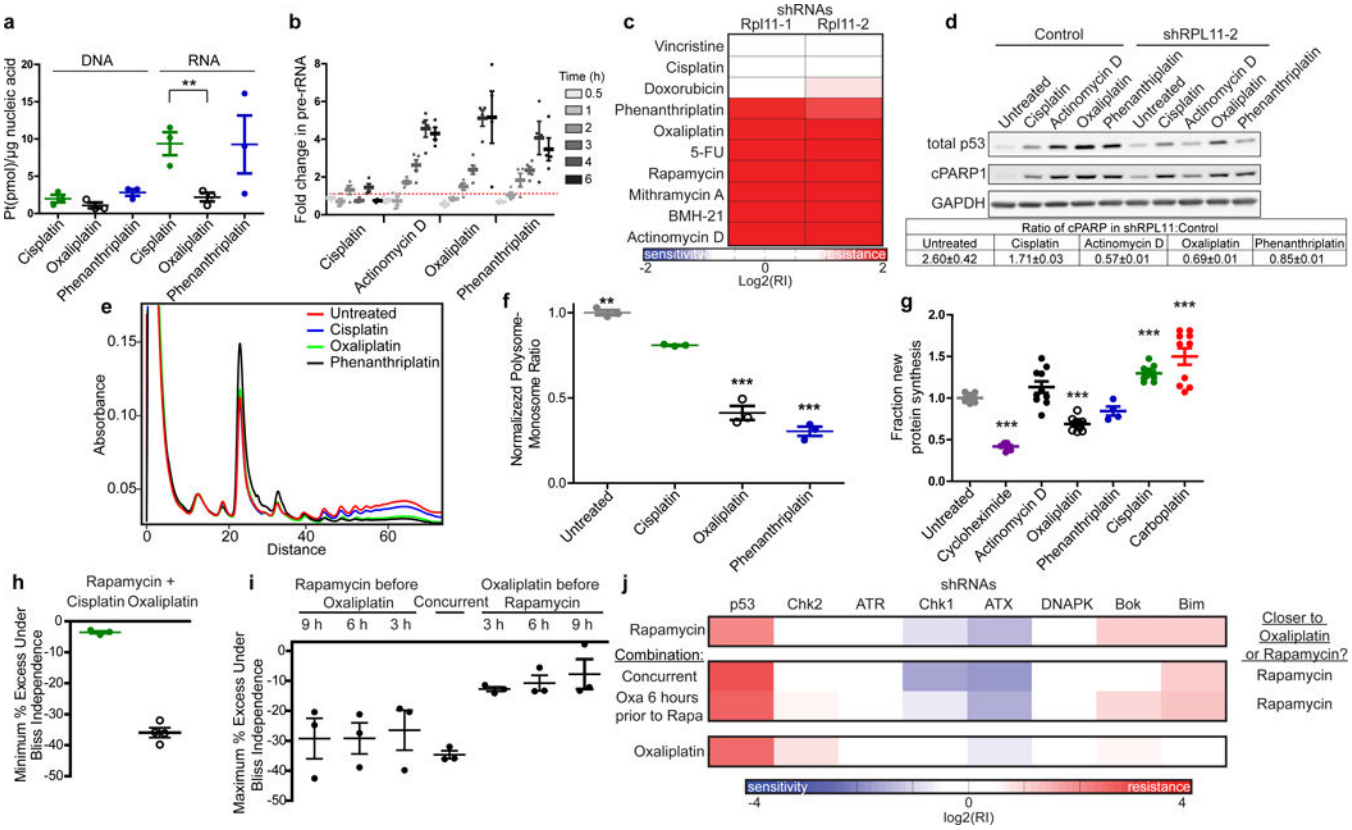

Figure 5.

Oxaliplatin and phenanthriplatin induce ribosome biogenesis stress. (**a**) Platinum per µg of nucleic acid as determined by atomic absorption spectroscopy as a result of 3 h of treatment of *Eu-Myc p19*$^{Arf-/-}$ lymphoma cells with cisplatin, oxaliplatin or phenanthriplatin at a concentration required to achieve LD80–90 at 48 h. Data are represented as mean ± SEM from three independent doses and cultures. $p < 0.005$ (**) by a two-tailed Student's t-test. (**b**) Percent of pre-ribosomal RNA at various time points after treatment of *Eu-Myc p19*$^{Arf-/-}$ lymphoma cells as determined by qPCR and normalized to GAPDH. Dashed red line indicates no change. Data are represented as mean ± SEM from four independent doses and cultures except 3 h which had five. (**c**) A heatmap depicting enrichment or depletion of two validated hairpins against RPL11 as a result of drug treatment in of *Eu-Myc p19*$^{Arf-/-}$ lymphoma cells. (**d**) Above: western blot for total p53, cleaved PARP (cPARP) and GAPDH 12 h after treatment with or without a hairpin against RPL11 in of *Eu-Myc p19*$^{Arf-/-}$ lymphoma cells. Below: densitometry quantification of cPARP. Shown is the ratio of cPARP in the shRPL11-2 condition relative to control for each treatment. Data are represented as mean ± SEM from three independent densitometry quantification results. (**e**) Representative polysome gradient after 6 h of treatment with the indicated agents *Eμ-Myc p19*$^{arf-/-}$ cells. (**f**) The ratio of polysomes to monosomes normalized to the untreated condition derived from the quantification of the area under the curve of monosome and polysome fractions. Data are represented as mean ± SEM from three technical dosing replicates. $p < 0.01$ (**) or $p < 0.001$ (***) for each group relative to cisplatin by one-way ANOVA with Dunnett's Multiple Comparison Test. (**g**) Fraction of newly synthesized protein relative to the untreated

condition for *Eu-Myc p19*$^{Arf-/-}$ lymphoma cells at 9 h as measured by O-propargyl puromycin incorporation. Data are represented as mean ± SEM. p < 0001 (***) for each group relative to untreated by one-way ANOVA with Dunnett's Multiple Comparison Test. All conditions were conducted with two independent doses on independent cultures. Number of fields analyzed was 11 for untreated, 10 for actinomycin D, oxaliplatin, cisplatin and carboplatin, 7 for cycloheximide and 4 for phenanthriplatin. (**h**) Minimum percent excess PI negative of *Eu-Myc p19*$^{Arf-/-}$ lymphoma cells under Bliss Independence, a control model of additivity, for the combination of rapamycin with either cisplatin or oxaliplatin. Data are represented as mean ± SEM from three independent doses on independent cultures. (**i**) Minimum percent excess PI negative cells under Bliss Independence, for the combination of rapamycin and oxaliplatin for which co-dosing was staggered as shown. Data are represented as mean ± SEM from three independent doses on independent cultures. (**j**) RNAi signatures for rapamycin or oxaliplatin, or the combination of the two dosed simultaneously or oxaliplatin 6 h prior to rapamycin. Both combination signatures were more similar to rapamycin than oxaliplatin.

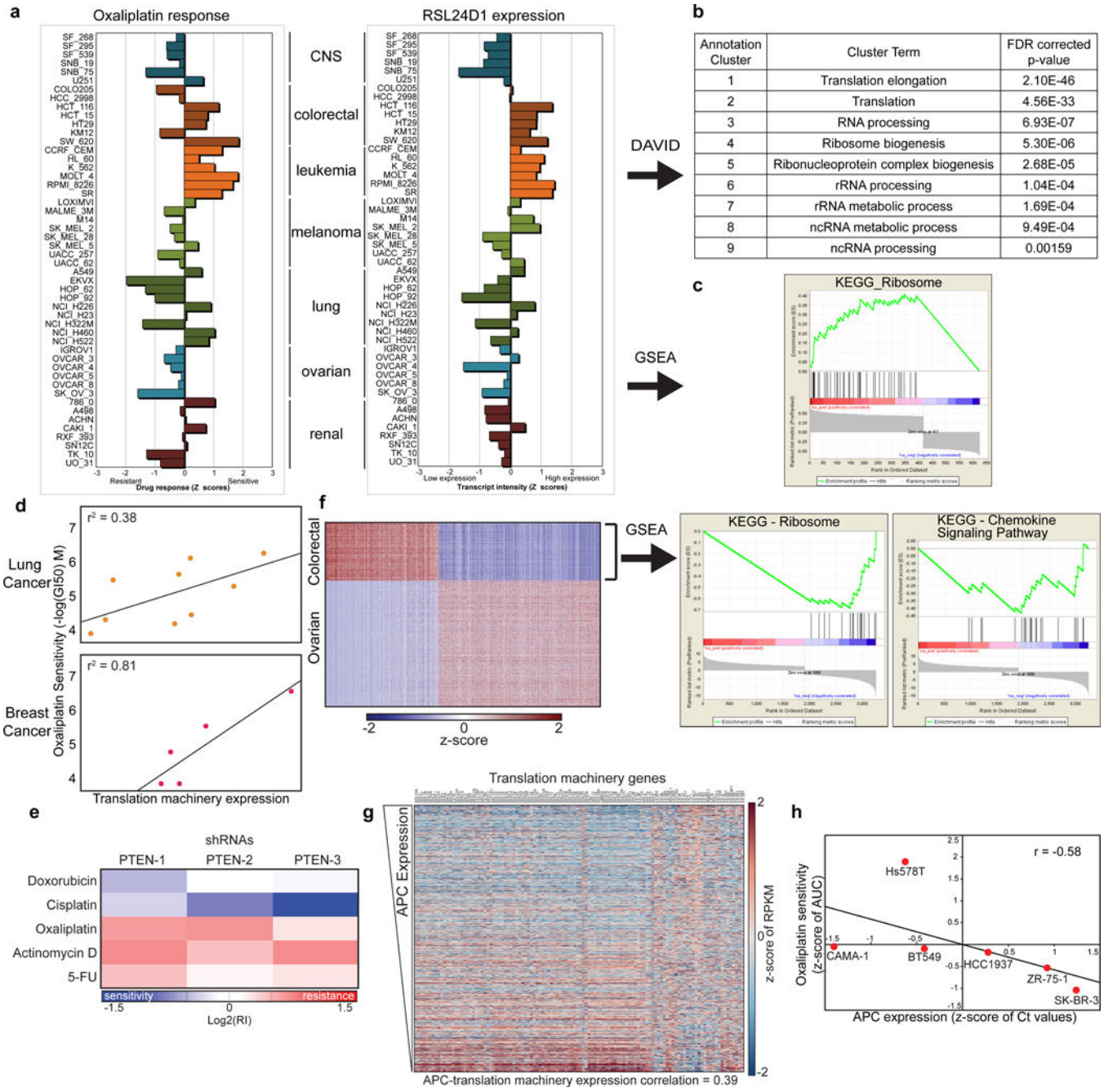

Annotation Cluster	Cluster Term	FDR corrected p-value
1	Translation elongation	2.10E-46
2	Translation	4.56E-33
3	RNA processing	6.93E-07
4	Ribosome biogenesis	5.30E-06
5	Ribonucleoprotein complex biogenesis	2.68E-05
6	rRNA processing	1.04E-04
7	rRNA metabolic process	1.69E-04
8	ncRNA metabolic process	9.49E-04
9	ncRNA processing	0.00159

Figure 6.

Evidence for sensitization to oxaliplatin in “translation addicted” cell lines and primary tumors. (**a**) Graphs of z-scores depicting relative resistance or sensitivity to oxaliplatin for various cell lines (left) or relative abundance of RSL24D1 transcript levels (right). (**b**) Gene ontology terms identified by DAVID as being significantly enriched among the 417 genes whose expression significantly correlated to oxaliplatin sensitivity. (**c**) The sole KEGG pathway identified by GSEA as being significantly enriched among the 417 genes whose expression significantly correlated to oxaliplatin sensitivity. (**d**) The correlation of the translation machinery metagene, an average of ~120 translation related gene transcripts, to

oxaliplatin sensitivity from the NCI-60 for lung and breast cancer cell lines. (**e**) A heatmap depicting enrichment or depletion of three validated hairpins targeting PTEN as a result of drug treatment of *Eu-Myc p19*$^{Arf-/-}$ lymphoma cells. (**f**) Left, a heatmap representing the relative expression of levels of all genes that are differentially expressed in ovarian cancer relative to colorectal cancer by an absolute fold change of at least $\log_2(2.5)$. Right, the two non-digestion/metabolism related KEGG pathways identified by GSEA as being significantly enriched among the genes whose expression was greater in colorectal cancer relative to ovarian cancer. (**g**) A heatmap of expression of translation machinery genes from the breast cancer TCGA dataset ranked by APC expression. (**h**) Breast cancer cell line sensitivity to oxaliplatin correlates to APC expression. Each dot is labeled according to the name of the cell line and represents the mean of three independent replicates of both the dosing and qPCR from the same culture.